Eur. Phys. J. B (2013) 86: 67
DOI: 10.1140/epjb/e2012-30730-9

THE EUROPEAN PHYSICAL JOURNAL B

Regular Article

Transport in a disordered tight-binding chain with dephasing

Marko Žnidarič[a] and Martin Horvat

Physics Department, Faculty of Mathematics and Physics, University of Ljubljana, 1000 Ljubljana, Slovenia

Received 7 August 2012 / Received in final form 21 August 2012
Published online 25 February 2013 –

Abstract. We studied transport properties of a disordered tight-binding model (XX spin chain) in the presence of dephasing. Focusing on diffusive behaviour in the thermodynamic limit at high energies, we analytically derived the dependence of conductivity on dephasing and disorder strengths. As a function of dephasing, conductivity exhibits a single maximum at the optimal dephasing strength. The scaling of the position of this maximum with disorder strength is different for small and large disorders. In addition, we studied periodic disorder for which we found a resonance phenomenon, with conductivity having two maxima as a function of dephasing strength. If the disorder is non-zero only at a random fraction of all sites, conductivity is approximately the same as in the case of a disorder on all sites but with a rescaled disorder strength.

1 Introduction

Understanding quantum transport in simple systems is of obvious relevance for understanding nano and mesoscopic devices as well as transport in real materials. One such model system is a tight-binding chain in the presence of disorder and dephasing, that was studied more than 30 years ago [1]. The goal is to understand the interplay of the disorder, incoherent processes and possibly interactions, on the transport properties. If the system is coherent, the procedure, at least in principle, is straightforward – one has to calculate the transmission by one of the various approaches, see for example, book [2] for an overview. Non-coherent processes due to interaction with external degrees of freedom, for instance, due to electron-phonon scattering, are more difficult to account for. Correspondingly, they are also less understood. In the present work we study the influence of the environment, in particular its dephasing effects, on the bulk quantum transport in a disordered system.

There are several approaches how to study incoherent transport. A rigorous one in terms of a non-equilibrium Green's function is difficult to analytically evaluate for all but the simplest systems, while its numerical calculation is very time-consuming and limited to small systems. With that in mind, alternative, more phenomenological approaches to incoherent transport are actively investigated. One of the earliest suggestions accounts for the dephasing by introducing fictitious reservoirs that break phase coherence [3]. This so-called Büttiker probe has been applied to the disordered tight-binding model [4] and is successfully used for the calculation of transmission through molecules, see references [5–8]. A phenomenological model of dephasing can also be constructed by using an appropriate self-energy in a non-equilibrium Green's function [9]. Another approach consists of treating the system as being composed of statistically distributed coherent and incoherent parts (having an imaginary self-energy) [10–12]. Dephasing can also be accounted for by simulating vibrational motion of individual sites [13], thereby modulating intersite couplings, as is for instance done using molecular dynamics simulations in carbon nanotubes [14].

In this paper we use a different approach by writing the quantum master equation of the Lindblad type [15,16] describing time evolution of the reduced density matrix of a tight-binding model without environment. Environmental dephasing is described in an effective way by dissipative operators that cause the decay of off-diagonal coherences (that is, also of the current). Coupling the system in addition to reservoirs, a true non-equilibrium steady state (NESS), reached after long time, is studied. Description with the Lindblad equation has its advantages and disadvantages. Compared to others, once NESS is found one has access to all many-body observables, that is to a complete state. Of course, this advantage can be harnessed only if one is able to solve the NESS. Fortunately, a tight-binding model with dephasing is solvable [17] in its Lindblad formulation. While a study of NESS' of Lindblad equations is a well-defined and important mathematical problem it has its down sides. A number of approximations, like weak coupling and fast-decaying bath correlations, are needed in standard derivations of the Lindblad equation [18]. We note, however, that the Lindblad master equation is expected to provide a good description on timescales that

[a] e-mail: znidaric@fmf.uni-lj.si

are much larger than the timescale of bath correlations. It namely provides the most general description for quantum processes that preserve, positivity, and, trace and form a dynamical semi-group. Memory effects, not accounted for by the Lindblad equation, are expected to be smaller at higher temperatures, which is the regime that we study. In addition, we are interested in the bulk transport properties in the thermodynamic limit for which finite-size boundary effects are expected to play no role. Compared to small systems, where more complicated master equations might be necessary for the correct description of transport, see for example [19], we can use simpler Lindblad equation to calculate bulk conductivity at high temperatures.

Tight-binding models with dephasing and disorder has also recently become of interest in the context of excitation transfer in biomolecules, in particular in photosynthetic complexes. There a coupling with the environment, that is, dephasing, increases the efficiency of excitation transfer because it counteracts localisation due to the disorder [20–24]. This, so-called environmentally assisted transport, can be, in long homogeneous chains explained by analytical results that we present.

Our study proceeds in two steps. First, using the method introduced in references [17,25] and extending it to an inhomogeneous system, we transform the problem from the state space of many-body density matrices, that is exponentially large in the chain length, to the one of two-point correlation functions, whose size is only quadratic in the chain length. We manage to analytically solve the resulting equations for some parameter regimes, while for other we resort to numerical solutions. In addition to explaining the dependence of conductivity, that is, of diffusion constant, on disorder and dephasing strength we also identify an interesting resonance phenomenon for periodically placed disorder.

2 XX chain with dephasing

We shall first present the model in the framework of Pauli matrices and show later a well-known fact that the model is equivalent to a non-equilibrium tight-binding model with an on-site disorder and dephasing due to the environment.

The Hamiltonian of the XX spin chain in an inhomogeneous magnetic field is given by

$$\mathcal{H} = \sum_{j=1}^{L-1} (\sigma_j^x \sigma_{j+1}^x + \sigma_j^y \sigma_{j+1}^y) + \sum_{i=1}^{L} \epsilon_i \sigma_i^z, \tag{1}$$

with standard Pauli matrices and L being the chain length. We use units in which $\hbar = 1$ and the nearest-neighbour hopping is $J = 1$. We shall describe evolution of the system, described by a many-body density matrix ρ of size 2^L, in the presence of the environment by Lindblad equation [15,16],

$$\frac{d}{dt}\rho = i[\rho, \mathcal{H}] + \mathcal{L}^{\mathrm{dis}}(\rho) \equiv \mathcal{L}(\rho), \tag{2}$$

in which dissipative influence of the environment is described by the so-called dissipator $\mathcal{L}^{\mathrm{dis}}$. The action of a dissipator on an arbitrary operator ρ is expressed in terms of Lindblad operators L_k as,

$$\mathcal{L}^{\mathrm{dis}}(\rho) = \sum_k \left([L_k \rho, L_k^\dagger] + [L_k, \rho L_k^\dagger] \right). \tag{3}$$

The dissipator will in our case consist of two parts, $\mathcal{L}^{\mathrm{dis}} = \mathcal{L}^{\mathrm{bath}} + \mathcal{L}^{\mathrm{deph}}$. The first $\mathcal{L}^{\mathrm{bath}}$ describes the action of two baths, one at each chain end, and will induce a non-equilibrium situation with the current flowing through the system. The bath is written as a sum of a part acting only at the left end (site index $j = 1$ and label "L") and a part acting only at the right end (site index $j = L$ and label "R"), $\mathcal{L}^{\mathrm{bath}} = \mathcal{L}_{\mathrm{L}}^{\mathrm{bath}} + \mathcal{L}_{\mathrm{R}}^{\mathrm{bath}}$. Two Lindblad operators at the left end are

$$L_1^{\mathrm{L}} = \sqrt{\Gamma(1+\mu)}\,\sigma_1^+, \quad L_2^{\mathrm{L}} = \sqrt{\Gamma(1-\mu)}\,\sigma_1^-, \tag{4}$$

while at the right end we have

$$L_1^{\mathrm{R}} = \sqrt{\Gamma(1-\mu)}\,\sigma_L^+, \quad L_2^{\mathrm{R}} = \sqrt{\Gamma(1+\mu)}\,\sigma_L^-, \tag{5}$$

$\sigma_j^\pm = (\sigma_j^x \pm i\,\sigma_j^y)/2$. The bath therefore flips the boundary spin up or down with certain probability. Parameter μ plays the role of the forcing, trying to induce magnetisation $+\mu$ at the left end and $-\mu$ at the right end[1]. The other dissipative part, $\mathcal{L}^{\mathrm{deph}}$, represents the influence of the environment at each site, being for instance, due to scattering on phonons. The dephasing part $\mathcal{L}^{\mathrm{deph}} = \sum_{j=1}^{L} \mathcal{L}_j^{\mathrm{deph}}$ is a sum of $\mathcal{L}_j^{\mathrm{deph}}$, each of which acts only at the jth site and is described by a single Lindblad operator,

$$L_j^{\mathrm{deph}} = \sqrt{\frac{\gamma}{2}}\sigma_j^z. \tag{6}$$

Due to dissipation the system's density matrix $\rho(t)$ will after a long time converge to a time-independent state $\rho_\infty \equiv \lim_{t\to\infty} \rho(t)$ which is called a non-equilibrium steady state (NESS). For our model the NESS ρ_∞ is unique and can be formally expressed via the solution of Lindblad equation (2) as $\rho_\infty = \lim_{t\to\infty} \exp(\mathcal{L}t)\rho(0)$. In this work we are interested in the NESSs bulk transport properties in the presence of disorder and dephasing. Conductivity is expected to be insensitive to details of bath Lindblad operators in the thermodynamic limit. All expectation values reported in the paper are with respect to the NESS state, that is $\langle A \rangle = \mathrm{tr}\,(A\rho_\infty)$.

As we are interested in transport properties, the central object we shall consider is the spin (that is, magnetisation) current j_r, defined at site r through a continuity relation, resulting in the expression $j_r \equiv \mathrm{i}\,[\sigma_r^z, \sigma_r^x \sigma_{r+1}^x + \sigma_r^y \sigma_{r+1}^y]$, giving

$$j_r = 2(\sigma_r^x \sigma_{r+1}^y - \sigma_r^y \sigma_{r+1}^x). \tag{7}$$

[1] Note that by having a non-zero average magnetisation in the driving, that is, a non-zero $\bar{\mu}$ in equations (7)–(8) of reference [25], there is only a shift in the overall magnetisation profile while having no effect on the remaining $L(L-1)$ two-point expectations studied in the present work.

Dephasing alone causes an exponential decay of off-diagonal matrix elements (in the standard basis in which σ^z is diagonal). Therefore, due to $\mathcal{L}^{\rm deph}(j_r) = -4\gamma j_r$, if there were no $\mathcal{H}$ and $\mathcal{L}^{\rm bath}$ in the Lindblad equation, dephasing would cause an exponential decay of current with time, $j_r(t) = \exp(-4\gamma t) j_r(0)$. In the presence of Hamiltonian and driving the evolution is more complicated, resulting in a nontrivial NESS. Evaluating the action (2) of dephasing (6) on the identity and σ^z operators, we see that $\mathcal{L}^{\rm deph}(\sigma_r^z) = \mathcal{L}^{\rm deph}(1_r) = 0$ hold.

3 Stationary solution

To find the NESS ρ_∞ we have to find a stationary solution of equation (2), that is, solve $\mathcal{L}(\rho_\infty) = 0$. Expanding ρ_∞ in an operator basis the stationary equation can be written as a set of coupled linear equations for unknown expansion coefficients. Because the number of unknown coefficients is $4^L - 1$, and therefore grows exponentially with the system size L, it is for a generic system impossible to analytically obtain ρ_∞. The XX model with dephasing, however, has a nice property that these exponentially many equations split into smaller sets of equations that are uncoupled [17,25–27]. Namely, there is a hierarchy of observables according to the number of fermionic operators they contain. For instance, all two-point observables decouple from the rest, meaning that one can write a closed set of equations for observables involving two fermionic operators. Once these are known, they can be used as a "source" term in equations for three-point observables, and so on for higher order correlations. For general consideration, when such a hierarchy appears, see references [26,28].

As shown in reference [17], one consequence of such a structure is that the NESS can be written as

$$\begin{aligned} \rho_\infty &= \frac{1}{2^L}\left[1 + \mu(H+B) + \mathcal{O}(\mu^2)\right] \\ H &= \sum_{r=1}^{L} \sum_{j=1}^{L+1-r} h_j^{(r)} H_j^{(r)} \\ B &= \sum_{r=2}^{L} \sum_{j=1}^{L+1-r} b_j^{(r)} B_j^{(r)}, \end{aligned} \tag{8}$$

where we define

$$H_j^{(r+1)} \equiv \sigma_j^x Z_{j+1}^{(r-1)} \sigma_{j+r}^x + \sigma_j^y Z_{j+1}^{(r-1)} \sigma_{j+r}^y$$

and

$$B_j^{(r+1)} \equiv \sigma_j^x Z_{j+1}^{(r-1)} \sigma_{j+r}^y - \sigma_j^y Z_{j+1}^{(r-1)} \sigma_{j+r}^x,$$

when $r \geq 2$ and with $Z_j^{(r)} \equiv \sigma_j^z \ldots \sigma_{j+r-1}^z$ being a string of r consecutive σ^z's. $H_j^{(1)}$ is defined as $H_j^{(1)} \equiv -\sigma_j^z$. Let us stress that equation (8) is not just a perturbative expansion in μ as it might seem at a first glance – it is an exact ansatz [17,25] holding for any driving μ. Or, in other words, terms proportional to μ^2 (and of higher order) not written explicitly in equation (8) are all orthogonal (using Hilbert-Schmidt inner product $\langle A, B\rangle \equiv \mathrm{tr}\,(A^\dagger B)$) to operators in H and B. Expectation value of these observables is therefore obtained exactly to all orders in μ by calculating only the expansion coefficients contained in H and B. In particular, noting that $H_r^{(2)}$ is a hopping contribution to the energy density, $B_r^{(2)}$ current and $H_r^{(1)}$ magnetisation, all quantities necessary to study transport are contained in the ansatz (8).

Writing now $\mathcal{L}(\rho_\infty) = 0$ using the ansatz (8), we get the aforementioned closed set of linear equations for unknown coefficients $h_j^{(r)}$ and $b_j^{(r)}$. These are

$$\begin{aligned} \Gamma + \Gamma h_1^{(1)} - b_1^{(2)} &= 0, \\ -\Gamma + \Gamma h_L^{(1)} - b_{L-1}^{(2)} &= 0, \\ b_j^{(2)} - b_{j+1}^{(2)} &= 0, \;\; j = 2, \ldots, L-2, \end{aligned} \tag{9}$$

and for $r \geq 2$

$$\begin{aligned} &(h_j^{(r-1)} - h_{j+1}^{(r-1)}) + (h_j^{(r+1)} - h_{j-1}^{(r+1)}) \\ &\qquad + (\epsilon_j - \epsilon_{j+r-1}) h_j^{(r)} + \Upsilon_j^{(r)} b_j^{(r)} = 0 \end{aligned}$$

$$\begin{aligned} &(b_j^{(r-1)} - b_{j+1}^{(r-1)}) + (b_j^{(r+1)} - b_{j-1}^{(r+1)}) \\ &\qquad + (\epsilon_j - \epsilon_{j+r-1}) b_j^{(r)} - \Upsilon_j^{(r)} h_j^{(r)} = 0, \end{aligned} \tag{10}$$

where $\Upsilon_j^{(r)} \equiv 2\gamma + \Gamma\delta_{j,1} + \Gamma\delta_{j+r-1,L}$. There are L^2 equations for exactly as many unknown coefficients. Solving equations (10) therefore gives exact expectation values of observables $H_j^{(r)}$ and $B_j^{(r)}$.

The set of equations (9) and (10) can be compactly written in a matrix form by defining a hermitian correlation matrix C of size $L \times L$ with matrix elements $C_{j,k} \equiv h_j^{(k-j+1)} + \mathrm{i}\, b_j^{(k-j+1)}$ for $k > j$, $C_{j,j} \equiv h_j^{(1)}$, while $C_{j,k} = C_{k,j}^*$ for $j > k$. Let us also define $A \equiv \mathrm{i}E - \mathrm{i}J + \Gamma R$, where E is a diagonal disorder matrix, $E_{j,j} = \epsilon_j$, while non-zero matrix elements of J are $J_{i,i+1} = 1, J_{i+1,i} = 1$, while R has only two non-zero elements, $R_{1,1} = R_{L,L} = 1$. All L^2 equations (9) and (10) can now be written as a single matrix equation,

$$AC + CA^\dagger + 2\gamma\tilde{C} = P, \tag{11}$$

where $P_{1,1} = -2\Gamma$, $P_{L,L} = 2\Gamma$, while all other elements of P are zero, and $\tilde{C} = C - \mathrm{diag}(C)$ is the correlation matrix without the diagonal. Physically, P represents the driving, E the disorder, R the coupling to baths, $\tilde{C}$ term the dephasing while J is due to XX Hamiltonian. Note that without dephasing, $\gamma = 0$, the matrix equation (11) would be of the Lyapunov type. Lyapunov equations appear in NESS solutions of quadratic systems, see for example [29,30].

Equation (11) is the starting point for our study. In some cases we are able to solve it analytically, in others we resort to numerically exact solutions using standard linear algebra packages that enable solution for chain lengths L of up to several thousand.

Expectation values of all operators $H_j^{(r)}$ and $B_j^{(r)}$ are trivially proportional to μ, see equation (8), and we

therefore without loss of generality from now on set $\mu = 1$. Coupling strength to reservoirs Γ in general influences boundary resistance. Because we are interested in the regime of diffusive bulk transport, for which the boundary resistance does not matter in the thermodynamic limit, we additionally set $\Gamma = 1$. For transport properties special attention shall be paid to the diagonal elements of the correlation matrix C, giving the magnetisation profile, and to the imaginary part of the first near-diagonal, $b_j^{(2)}$, giving the current. Note that the current is due to equation (9) independent of the site index; henceforth we shall frequently use a shorter notation $b \equiv b_j^{(2)}$, resulting in spin current expectation value $\langle j \rangle = 4b$. Spin conductivity (depending on the context also called the diffusion constant), being a proportionality constant between the gradient of a driving field, in our case magnetisation, and a current, is therefore $\kappa = \lim_{L\to\infty} \frac{L\langle j_k\rangle}{\langle \sigma_L^z - \sigma_1^z\rangle} = \lim_{L\to\infty} 2Lb$. Here we used the thermodynamic limit $\langle \sigma_L^z - \sigma_1^z\rangle \to 2$ (for $\mu = 1$). We see that the conductivity is finite and non-zero, that is, we have a diffusive transport, provided the current scales as $j \sim 1/L$.

Let us finally briefly discuss the energy range to which the studied NESS states correspond. We prefer to use energy instead of temperature because thermalisation in integrable systems, of which the XX chain is an example of, can depend on the choice of Lindblad reservoirs [31]. There are two contributions to the energy (1), hopping and magnetisation. As we shall see, the average magnetisation profile is linear. Each individual term $\epsilon_i \sigma_i^z$ will have fluctuations of order $\sim \sigma\mu$ centred around zero, meaning that their sum gives negligible contribution to the energy density in the thermodynamic limit. A similar conclusion holds for $\sigma_j^x \sigma_{j+1}^x + \sigma_j^y \sigma_{j+1}^y$. Namely, such term is essentially given by $\approx b_j^{(2)}(\epsilon_j - \epsilon_{j+1})/\gamma$ (see for example Eq. (A.3)), again giving negligible contribution to the energy density in the thermodynamic limit. Therefore, in the thermodynamic limit the NESS solution (8) is always close to the identity matrix (that is, an infinite temperature state). This means that we are studying transport properties at high energies.

4 Fermionic picture

It is helpful to translate quantities from the spin language of Pauli matrices to the fermionic language of creation $c_j^\dagger$ and annihilation c_j operators, satisfying anticommutators $\{c_j, c_k\} = 0$, $\{c_j^\dagger, c_k^\dagger\} = 0$, and $\{c_j, c_k^\dagger\} = \delta_{j,k}1$. Using Jordan-Wigner transformation [32], $c_j = -(\sigma_1^z \dots \sigma_{j-1}^z)\sigma_j^+$, or its inverse, $\sigma_j^x = -(\sigma_1^z \dots \sigma_{j-1}^z)(c_j + c_j^\dagger)$, $\sigma_j^y = -\mathrm{i}(\sigma_1^z \dots \sigma_{j-1}^z)(c_j - c_j^\dagger)$, and $\sigma_j^z = c_j c_j^\dagger - c_j^\dagger c_j = 1 - 2n_j$, where we denote by $n_j = c_j^\dagger c_j$ a number operator at site j, the Hamiltonian (1) can be rewritten as a nearest-neighbour hopping,

$$\mathcal{H} = \sum_j 2(c_j^\dagger c_{j+1} - c_j c_{j+1}^\dagger) + \sum_i \epsilon_i (1 - 2n_i). \qquad (12)$$

Random magnetic fields ϵ_i translate to a diagonal on-site disorder. Spin current j_r translates to $j_r = 4\mathrm{i}(c_r^\dagger c_{r+1} + c_r c_{r+1}^\dagger)$, that is, is proportional to the particle current. Bath Lindblad operators (4) on the other hand inject or absorb a particle, thereby inducing non-zero particle current through the system. Operators $H_j^{(r)}$ and $B_j^{(r)}$ in the ansatz (8) translate for $r \geq 2$ to

$$\begin{aligned} H_j^{(r+1)} &= 2(c_j^\dagger c_{j+r} - c_j c_{j+r}^\dagger) \\ B_j^{(r+1)} &= 2\mathrm{i}(c_j^\dagger c_{j+r} + c_j c_{j+r}^\dagger). \end{aligned} \qquad (13)$$

They are two-point operators involving two fermions. Coefficients in the correlation matrix C (11) therefore give expectation values of all two-point functions in the fermionic picture. In particular, the density profile is $\langle n_j \rangle = (1 + h_j^{(1)})/2$, while the particle (charge) current $j_k^{(n)}$ is defined as $j_k^{(n)} = 2i\,[n_k, c_k^\dagger c_{k+1} - c_k c_{k+1}^\dagger] = B_k^{(2)}$, has an expectation value,

$$j \equiv \langle j_k^{(\mathrm{n})} \rangle = 2b. \qquad (14)$$

Conductivity in the fermionic picture is therefore

$$\kappa = \lim_{L\to\infty} \frac{L\langle j_k^{(\mathrm{n})}\rangle}{\langle n_L - n_1\rangle} = \lim_{L\to\infty} L2b, \qquad (15)$$

and is the same as in spin language. In most of figures we shall either show the dependence of particle current $j_k^{(\mathrm{n})}$, simply denoted by j, or of conductivity κ.

5 Homogeneous disorder

In this section we study the simplest case in which the disorder is present at each site and has the same variance. Each ϵ_j is an independent random variable with a uniform distribution $p(w) = \text{const.}$ in the interval $w \in [-\sqrt{3}\sigma, \sqrt{3}\sigma]$. We therefore have disorder averaged values $\langle \epsilon_j \rangle = 0$ and $\langle \epsilon_j^2 \rangle = \sigma^2$. Our results do not depend on details of the distribution $p(w)$, only on its width σ. Also, a homogeneous non-zero average $\langle \epsilon_j \rangle$ would not change any of the results presented, see discussion in reference [25].

In the next subsection we shall first study the case without dephasing for which one has Anderson localisation (in the master equation setting). This regime is studied to set the relevant length scale of localisation. New results about the interplay of dephasing and disorder are then presented in subsequent Section 5.2.

5.1 Localised phase, $\gamma = 0$

Without dephasing, $\gamma = 0$, we have an ordinary tight-binding model with diagonal disorder in a non-equilibrium setting. One expects that Anderson localisation [33] of the conservative model, for which in 1D all eigenstates of $\mathcal{H}$ are localised, will be reflected in an exponential decay of current with length L (at constant driving). This has

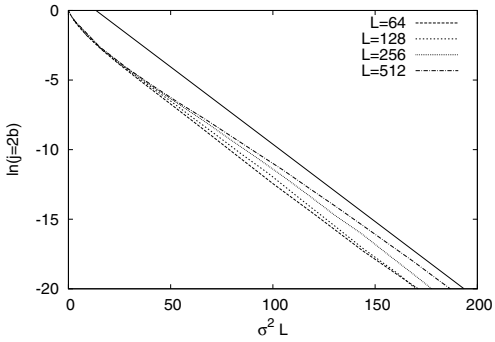

Fig. 1. An ensemble averaged logarithm of the particle current for different chain lengths $L = 64, 128, 256, 512$ (bottom to top) and disorder strengths σ, all for $\gamma = 0$. We have a universal exponential decay due to localisation, $\ln j \sim(-L/l)$, with localisation length $l \approx 9/\sigma^2$ (solid line above numerical curves). Non-asymptotic behaviour for $\sigma^2 L \lesssim 10$ is due to localisation length being larger than L.

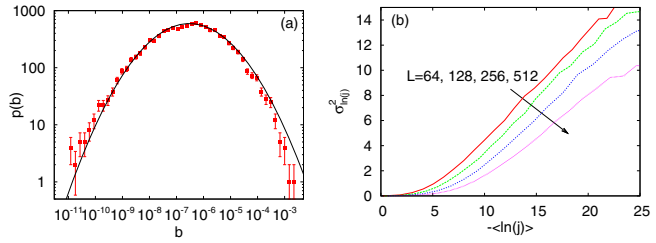

Fig. 2. (Color online) (a) Distribution of particle current (points) is close to log-normal (full curve). All is for $L = 128$, $\sigma = 1$. (b) Dependence of the variance of $\ln j$ on its average. Both plots are for zero dephasing, $\gamma = 0$.

been numerically observed in reference [34]; here we determine the decay rate, that is, the localisation length, due to its importance as a length scale which is also relevant when $\gamma \neq 0$. In Figure 1 we can see that the localisation length determined from the dependence of current scales as $l \approx 9/\sigma^2$, and is consistent with previous similar observations in a non-equilibrium setting [10].

It is known from early studies of the Anderson model [35] that the distribution of current is log-normal, that is, distribution of its logarithm is normally distributed, away from band edges. For log-normal distribution the average current can be expressed as $\langle j\rangle = \exp(m + s^2/2)$, where $m = \langle \ln j\rangle, s = \sigma_{\ln j}$. The question of conductance distribution in the Anderson model at the band centre or at the band edge however is a rather delicate one. Namely, an otherwise universal single-parameter scaling theory [36], saying essentially that the distribution function of conductance is a function of a single parameter (say of its first moment), is modified in the band centre [11,37,38]. We can see in Figure 2 that in our non-equilibrium setting the distribution of current is almost log-normal. The single-parameter scaling relation between the first two moments of $\ln j$ on the other hand does not hold. Whether small discrepancies visible in the decay of current in Figure 1 are due to the band-centre anomaly is not clear.

5.2 Diffusive regime for non-zero dephasing

We proceed to the main part of our work, that is to the case of non-zero dephasing γ. Relevant parameters are disorder strength σ, dephasing strength γ and the chain length L. Fixing σ and $\gamma > 0$, we find that the current always scales diffusive as $j \sim 1/L$ for sufficiently long chains. That is, in the thermodynamic limit a non-zero dephasing always causes the system to become diffusive, regardless of whether it was ballistic (for $\sigma = 0$) or localised (for $\sigma \neq 0$) without dephasing. We note that interaction between particles still preserves the diffusive nature of transport [34]. We shall only discuss properties in the thermodynamic limit, that is in the regime when the system is diffusive. For finite size effects that appear in the transition region from a localised/ballistic phase for small L's to a diffusive phase see Appendix C.

We first focus on the case of large disorder σ. For large σ the size of $|C_{j,j+r}|$ exponentially decreases with the distance r from the diagonal (we will see that this holds also for large γ). In the extreme case we can therefore approximate C with a tridiagonal matrix: we assume that the only non-zero elements of C are on the diagonal and in the first off-diagonal. Doing this approximation, equation (11) can be solved exactly for any L, σ and γ, see Appendix A. In the thermodynamic limit the expression for b is

$$b = \frac{\gamma}{L}\frac{2}{2\gamma^2 + \sigma^2}, \tag{16}$$

immediately giving conductivity (15),

$$\kappa = \frac{2}{\gamma + \frac{\sigma^2}{2\gamma}}. \tag{17}$$

Expression of the same form has been obtained in reference [23] when studying time-evolution in a single-particle sector of a tight-binding model. Analogous formulas for the diffusion constant have been obtained before in the context of spreading of particles in the electric field [39,40], where the role of the disorder strength is played by the Bloch oscillation frequency.

Transport properties in condensed-matter systems are discussed many times in terms of scattering lengths. Heuristically, one often assumes that different scattering processes are independent and that one can simply sum-up scattering rates, that is, reciprocal scattering lengths. Interpreting analytical result for conductivity (17) in such a way one can say that the total scattering length $l_{\rm tot}$ has an independent contribution from dephasing $l_{\rm deph} = 1/\gamma$ and disorder $l_{\rm dis} = 2\gamma/\sigma^2$, giving $1/l_{\rm tot} = 1/l_{\rm deph} + 1/l_{\rm dis}$ with $\kappa \propto l_{\rm tot}$. This of course holds only in the regime of the validity of equation (17), that is for large σ or large γ.

In Figure 3 we can see that formula (17) agrees well with numerical results for large σ. Two gross features are

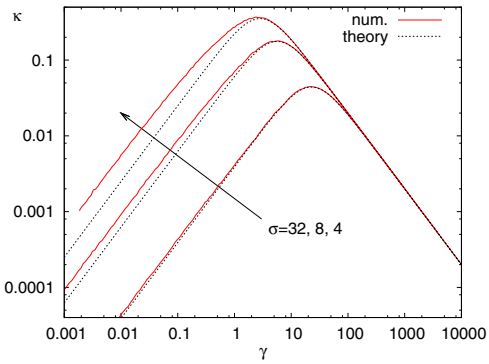

Fig. 3. (Color online) Dependence of conductivity κ on dephasing strength γ for large disorder σ. Numerical results (full red curve) agree well with theoretical formula, equation (17) (dotted curves).

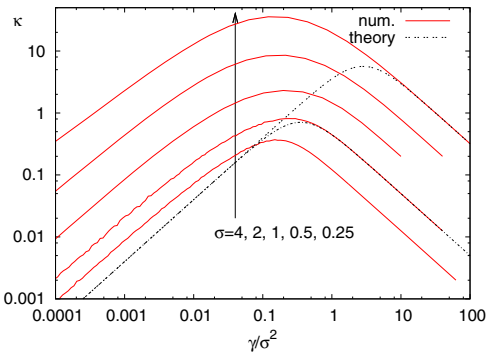

Fig. 4. (Color online) Conductivity at a smaller disorder. Large-σ theory (dotted curves), equation (17), still works for sufficiently large dephasing $\gamma \gtrsim \sigma$.

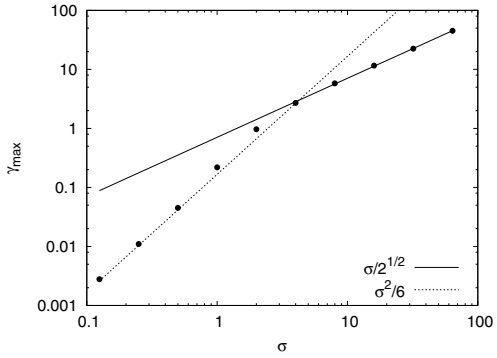

Fig. 5. Location of the maximum $\gamma_{\max}$ in $\kappa(\gamma)$ as a function of disorder strength σ. Lines show asymptotic theoretical scaling, having two regimes, points are numerics.

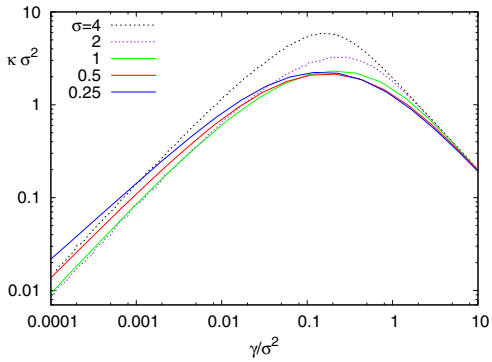

Fig. 6. (Color online) Scaled conductivity κ for small disorder σ.

visible: (i) $\sim 1/\gamma$ dependence of κ for large dephasing – as the dephasing becomes large, scattering due to impurities can be neglected, and (ii) for small dephasing the transport is dominated by a break-down of localisation caused by non-zero dephasing; correspondingly, κ increases with the dephasing. A combined effect of the two contributions causes a maximum in conductivity at an intermediate dephasing strength. Similar behaviour has been observed in other studies [1,10–12] of dephasing effects on transport in a disordered tight-binding model as well as in transport properties of molecules or molecular aggregates [7,8,20,21,24,41]. The location of the maximum in κ scales according to (17) as $\gamma_{\max} = \sigma/\sqrt{2}$, with the value of κ at the maximum being $\kappa_{\max} = 2/(\sigma\sqrt{2}) = 1/\gamma_{\max}$. Around $\sigma \approx 4$ and smaller, appreciable differences between numerical results and the theoretical equation (17) are visible. The reason for this failure at smaller σ is that the approximation of the correlation matrix by a tridiagonal matrix becomes increasingly poor. For even smaller σ it completely fails. Numerical results in this regime of σ are shown in Figure 4. As opposed to large σ, the location of the maximum in the regime of small σ scales as $\gamma_{\max} \sim \sigma^2$ (Fig. 4), while the conductivity at the maximum is $\kappa_{\max} \sim 1/\sigma^2 \sim 1/\gamma_{\max}$. We see that the scaling of $\gamma_{\max}$ changes with σ. This can be nicely seen in Figure 5. The crossover between the two asymptotic behaviours happen around $\sigma \approx 3$. We observe that this coincides with the disorder strength at which localisation length for $\gamma = 0$ becomes $l \approx 1$.

Also, observe in Figure 4 that formula (17) still holds for sufficiently large γ, that is, for dephasing larger than about $\approx\sigma$. For $\gamma < \sigma$ and small σ, where (17) does not work anymore, we were not able to obtain theoretical prediction for the current and κ. Including more than three diagonals in the calculation does not bring a significant improvement on equation (17). It seems that the problem is in this regime strongly dominated by fluctuations and all elements of C have to be taken into account. Perturbation theory in either γ or σ is also not successful, see discussion at the end of Appendix C. In Figure 6 we show in more detail this small-σ behaviour. We can see that the dependence on γ is rather complicated to the left of the maximum at $\gamma_{\max}$. Overall, κ scales as $\sim 1/\sigma^2$, and is almost a function of the scaled variable γ/σ^2. Scaling though is not perfect (see the region left of the maximum), perhaps pointing to a nontrivial (non-additive) interplay of dephasing and disorder. Whether this complicated behaviour for small σ is in any way related to anomalous properties of the Anderson model at the band centre [42,43] (that is, at zero energy) for weak uncorrelated disorder remains to be explored. Our Lindblad reservoirs namely induce a NESS with energy close to 0, that is, in the band centre.

6 Diluted disorder

In this section we discuss the case when disorder is absent at some sites. Such situation of a diluted disorder is relevant for real materials that can be prepared with different concentrations of impurities. In theory, it is known that in a Hamiltonian system non-homogeneous disorder, for instance a correlated one, can have a profound effect on the Anderson localisation. In 1D correlations in disorder can namely cause a delocalisation, for example [44,45]. It is also worth mentioning that the band centre can be special in terms of localisation properties for weak (uncorrelated) diagonal [42,43] as well as for off-diagonal disorder [46,47].

We shall study two cases: (i) randomly placed diluted disorder in which a fraction p of randomly chosen sites have a disorder, and (ii) periodically placed disorder for which the disorder is placed at every λth site. We will see that the transport properties of case (i) are very similar to the case of a homogeneous disorder with a renormalised disorder strength $\sqrt{p}\sigma$. Case (ii) though is qualitatively different. Disorder distribution function shall in all cases be the same uniform distribution as before.

Before going to the properties of non-equilibrium states we briefly comment on the localisation properties of a corresponding conservative system. The eigenvalues and eigenstates of a tri-diagonal matrix describing a tight-binding model with disorder at randomly placed fraction p of sites were calculated and in case (i) all eigenstates were still localised. Their localisation length though differs. A fraction p of the eigenstates have localisation length that is the same as if the disorder were on every site, while $(1-p)L$ eigenstates have a larger localisation length and are clustered around the band centre at $E = 0$. For periodic disorder, case (ii), delocalised states appear at the band centre [48]. We found that all eigenstates with eigenenergies $|E| \lesssim \frac{1}{L\sigma}$ (for $\lambda = 2$) were delocalised. Such delocalised eigenstates cause the spreading of initial localised packets as can be seen in Figure 7. We expect that this fraction $\sim 1/L$ of all eigenstates will strongly influence transport properties out of equilibrium if dephasing is zero or small.

6.1 Randomly placed diluted disorder

From the tri-diagonal derivation in Appendix A, holding for large γ, we see that the fact that disorder is not present at each site will be reflected in an additional prefactor in front of σ^2. Instead of $L\sigma^2$ as for the homogeneous case we will have $pL\sigma^2$, resulting in the conductivity

$$\kappa = \frac{2}{\gamma + p\frac{\sigma^2}{2\gamma}}. \tag{18}$$

The equation is the same as would be for the homogeneous case with an effective disorder strength $\sigma_{\rm ef} = \sqrt{p}\sigma$. This expression is expected to be valid for large γ. For smaller dephasing, even though we do not have a theoretical formula, we can still try to approximate the diluted situation with a homogeneous one at the effective disorder strength inferred from large γ behaviour (18). In Figure 8 we compare results for a diluted disorder with the ones for a homogeneous case with a smaller effective disorder. The agreement between κ for a randomly diluted disorder and a homogeneous one with a rescaled effective disorder is not perfect to the left of the maximum.

That for diluted disorder, the disorder strength is just renormalised is not very surprising. Such a result follows from the assumption that scattering events are independent and therefore the scattering length scales as $\sim 1/p$. Scaling of such form has been observed experimentally in 1D spin chain materials described by the isotropic Heisenberg model in which scattering events are due to impurities [49]. We expect that findings of the present manuscript for the XX chain would not qualitatively change in the presence of interaction, that is, for the Heisenberg model.

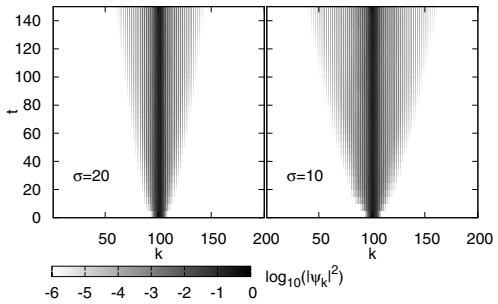

Fig. 7. Wave-packet spreading in the case of periodic disorder ($\lambda = 2$). Vertical axis is time, horizontal axis is the spatial position within a system of length $L = 200$. Due to a fraction of delocalised states the packet, initially localised around $k = 100$, spreads with time. Two different disorder strengths shown as $\sigma = 20$ and $\sigma = 10$, result in different speeds of spreading. Note that the amplitude of the spreading part of a wavepacket is small (grayscale is logarithmic).

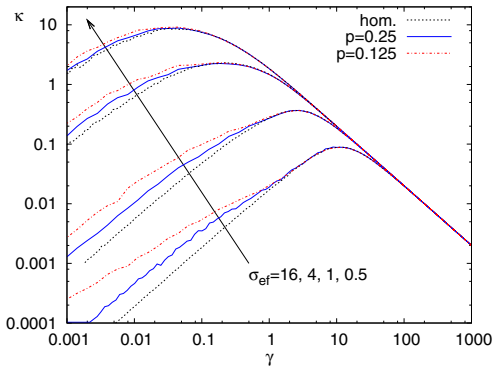

Fig. 8. (Color online) Conductivity for a diluted disorder. Disorder is placed on random pL sites. Black dotted curves are for a homogeneous disorder ($p = 1$) with strength $\sigma_{\rm ef}$, blue and red are for a diluted case with $\sigma = \sigma_{\rm ef}/\sqrt{p}$.

6.2 Periodic disorder

In this subsection we place disorder of strength σ at every λth site, that is, at sites $j = k\lambda - 1, k \in \mathbb{N}$, while there is no disorder at any other sites.

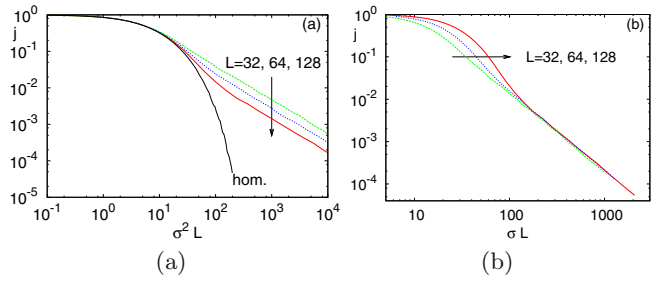

Fig. 9. (Color online) Periodic disorder with period $\lambda = 2$ and $\gamma = 0$. Scaling of the particle current j with σ for $L = 32, 64, 128$. Difference between (a) and (b) is only in the scaling on the x-axis. (a) For $L\sigma^2 \lesssim 10$ (when localisation length l is larger than L) periodicity is irrelevant and the dependence is the same as for a homogeneous disorder with a rescaled disorder strength $\sigma/\sqrt{2}$ at every site (black solid curve "hom."; the same exponentially localised data as in Fig. 1). Scaling variable is $\sigma^2 L$. (b) For larger disorders the scaling variable is σL and the decay is algebraic, $j \sim 1/(L\sigma)^\alpha$ with $\alpha \approx 2$.

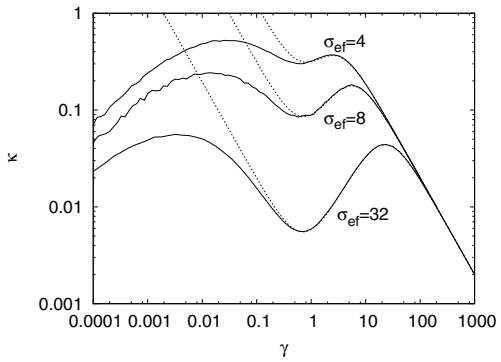

Fig. 10. Conductivity for disorder on every second site (full curves) and the theoretical equation (21) (dotted curves).

First, we check conductivity for $\gamma = 0$. The results from solving equation (11) and averaging over the disorder are shown in Figure 9. For sufficiently small disorder σ, such that the localisation length l is larger than L, the dependence of current j on σ is the same as for a homogeneous disorder with a renormalised disorder strength of size $\sigma\sqrt{1/\lambda}$. One can see in Figure 9a that the differences between an exponentially localised homogeneous case and the periodic case begin to appear only for $\sigma^2 L \gtrsim 10$. For a larger disorder, when periodicity becomes important, the nature of decay with L changes (Fig. 9b). Current begins to decay in an algebraic way as $j \sim 1/L^2$. Such decay can be traced back to properties of the Hamiltonian system, which has a fraction $1/L$ of delocalised eigenstates having eigenenergies of order $\sim 1/L$ located around the band centre.

We next move to non-zero dephasing for which the transport is always diffusive in the thermodynamic limit. System size at which this diffusive behaviour is reached is larger than in the homogeneous case and depends on σ and γ. The main difference with respect to the homogeneous or randomly diluted case is that the dependence of $\kappa(\gamma)$ has two peaks. An additional resonant peak appears at smaller γ for a sufficiently large disorder σ, see Figure 10. While the right peak is correctly described by equation (18) with $p = 1/\lambda$, we have not been able to theoretically describe the left peak. Empirically we find that its position is

$$\gamma_1 \approx 1/(3\lambda\sigma). \tag{19}$$

Note that the position of the right peak is due to equation (18)

$$\gamma_2 = \sigma/\sqrt{2\lambda}. \tag{20}$$

The left peak is essentially a resonant phenomenon while the right one is due to competition between disorder and dephasing. Heuristically, γ_1 can be explained as the dephasing strength at which the dephasing time $1/\gamma$ is equal to the time a ballistic disturbance with speed v needs to travel a distance λ. We have seen in Figure 7 that for periodic disorder there are indeed delocalised eigenmodes in the absence of dephasing, with their speed being inversely proportional to σ, $v \sim 1/\sigma$. A resonant condition is therefore $1/\gamma \sim \lambda/v \sim \lambda\sigma$, resulting in equation (19).

Even though we are not able to theoretically describe the left peak we can derive the location of the minimum between the two peaks. Assuming that non-zero elements of C are only on the diagonal and two off-diagonals ($b^{(2)}, h^{(2)}$ and $b^{(3)}, h^{(3)}$), we can solve b, see Appendix B. The result is in the thermodynamic limit

$$b = \frac{1}{L\gamma(1 + \frac{\sigma_{\rm ef}^2}{2\gamma^2+1})}, \tag{21}$$

where $\sigma_{\rm ef} = \sigma/\sqrt{\lambda}$. Note that the difference from the 3-diagonal approximation (16) is only in the number 1 in the denominator. One can see in Figure 10 that equation (21) correctly describes the minimum. Location of the minimum is at $4\gamma_{\rm min}^2 = \sigma_{\rm ef}^2 - 2 - \sigma_{\rm ef}\sqrt{\sigma_{\rm ef}^2 - 8}$; this minimum is real for $\sigma_{\rm ef} > \sqrt{8} \approx 2.83$ while its location goes toward $\gamma_{\rm min} \asymp \sqrt{3}/2 \approx 0.73$ for large σ. We therefore expect the left resonant maximum at γ_1 to appear only for $\sigma \gtrsim 3$ which is indeed confirmed by numerical calculations shown in Figure 11. From equation (21) we also see the height at the minimum scales as $\asymp 1/\sigma^2$. To also describe the maximum, and not just the minimum, we would have to solve at least the diagonal and 4 off-diagonals in C, which proves to be too difficult (resonant maximum also appears only for chains with $L \geq 5$). In Figure 11 we can see that location of the two maxima is nicely predicted by equations (19) and (20). Dependence of κ for periodic disorder, having two maxima, can be compared to the one for randomly placed disorder (with the same average density), for which only the right maximum is present, see Figure 12.

7 Conclusion

We have studied conductivity in a tight-binding model with on-site disorder and experiencing dephasing. Transport is induced by a non-equilibrium driving described by

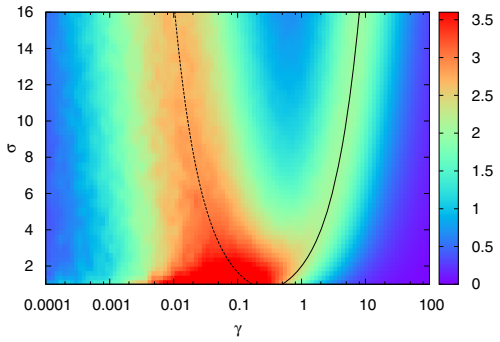

Fig. 11. (Color online) Density plot of a scaled conductivity $\sigma\,\kappa$ as a function of γ and σ for disorder on every $\lambda = 2$ site ($L = 256$). We multiply conductivity by σ in order to have a better contrast for two peaks. Two black curves denote position of the maxima, left curve equation (19), and right curve equation (20).

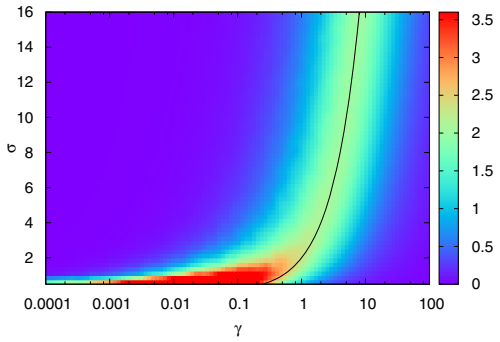

Fig. 12. (Color online) Scaled conductivity $\sigma\kappa$ as a function of γ and σ for disorder at half the sites which were randomly chosen ($p = 0.5$, $L = 256$). The black curve is the theoretical prediction for the location of the maximum at large σ, equation (20) with $\lambda = 2$.

the Lindblad master equation. Writing linear system of equations for all two-point fermionic expectation values in the steady state we study dependence of conductivity on dephasing and disorder strength. For large disorder or large dephasing we derive an analytic expression showing that the conductivity has a single maximum as a function of dephasing. We also discuss the case of diluted disorder. For randomly placed diluted disorder conductivity is approximately the same as for a homogeneous disorder with a rescaled disorder strength. For periodically placed disorder though a second resonant maximum in conductivity appears, exhibiting different scaling on parameters as the first maximum.

We acknowledge support by the grant P1-0044.

Appendix A: 3-diagonal approximation

For large disorder σ (and any γ) or for large γ the size of correlations $|C_{j,j+r}|$ rapidly decreases away from the diagonal, that is, one has $|C_{j,j+r}| \sim \exp(-r/\rho)$ with small ρ. In such a case one can approximate C by its diagonal $C_{j,j}$ and its two nearest diagonals, $C_{j,j+1}$, $C_{j+1,j}$. Setting all other matrix elements of C to zero one can solve equation (11) exactly as follows.

We use standard notation for the unknown terms in C, $h_j^{(1)} \equiv C_{j,j}$, $b \equiv \mathrm{Im}(C_{j,j+1})$ and $h_j^{(2)} \equiv \mathrm{Re}(C_{j,j+1})$. Two nontrivial equations (11) on the diagonal are

$$\begin{aligned} 2\Gamma h_1^{(1)} - 2b &= -2\Gamma \\ 2\Gamma h_L^{(1)} + 2b &= 2\Gamma, \end{aligned} \tag{A.1}$$

while off-diagonal we have imaginary parts,

$$\begin{aligned} b\,k + (h_1^{(1)} - h_2^{(1)}) + h_1^{(2)}(\epsilon_1 - \epsilon_2) &= 0 \\ 2b\gamma + (h_2^{(1)} - h_3^{(1)}) + h_2^{(2)}(\epsilon_2 - \epsilon_3) &= 0 \\ &\vdots \\ 2b\gamma + (h_j^{(1)} - h_{j+1}^{(1)}) + h_j^{(2)}(\epsilon_j - \epsilon_{j+1}) &= 0 \\ &\vdots \\ b\,k + (h_{L-1}^{(1)} - h_L^{(1)}) + h_{L-1}^{(2)}(\epsilon_{L-1} - \epsilon_L) &= 0, \end{aligned} \tag{A.2}$$

where $k \equiv \Gamma + 2\gamma$, and real part,

$$\begin{aligned} -kh_1^{(2)} + b(\epsilon_1 - \epsilon_2) &= 0 \\ -2\gamma h_2^{(2)} + b(\epsilon_2 - \epsilon_3) &= 0 \\ &\vdots \\ -2\gamma h_j^{(2)} + b(\epsilon_j - \epsilon_{j+1}) &= 0 \\ &\vdots \\ -kh_{L-1}^{(2)} + b(\epsilon_{L-1} - \epsilon_L) &= 0. \end{aligned} \tag{A.3}$$

To get the coefficient of the current b we sum all equations (A.2), and use the relation $h_1^{(1)} - h_L^{(1)} = 2(b - \Gamma)/\Gamma$ obtained from (A.1). This gives

$$b(2k + (L-3)2\gamma) + \sum_{j=1}^{L-1} h_j^{(2)}(\epsilon_j - \epsilon_{j+1}) + \frac{2}{\Gamma}(b - \Gamma) = 0. \tag{A.4}$$

It is worth pointing out that equation (A.4) holds true in general, not just in the case of a 3-diagonal approximation. Inserting into this relation expressions for $h_j^{(2)}$ obtained from equations (A.3), we get

$$b = \frac{2\gamma}{c + 2\gamma^2(L-1) + \sum_{j=2}^{L-2}(\epsilon_j - \epsilon_{j+1})^2/2}, \tag{A.5}$$

with the boundary term c being independent of the length L, $c = 2\gamma(\Gamma + \frac{1}{\Gamma}) + \frac{\gamma}{\Gamma+2\gamma}\left[(\epsilon_1 - \epsilon_2)^2 + (\epsilon_{L-1} - \epsilon_L)^2\right]$.

Let ϵ_j be distributed according to a distribution having a finite second moment, $\langle \epsilon_j^2 \rangle = \sigma^2$. Then $\epsilon_j - \epsilon_{j+1}$ has second moment equal to $2\sigma^2$. According to the central limit theorem a sum of terms $(\epsilon_j - \epsilon_{j+1})^2$ will converge to a Gaussian distributed random variable with a non-zero average $2(L-3)\sigma^2$ and a variance $\propto L$. Expression $\sum_{j=2}^{L-2}(\epsilon_j - \epsilon_{j+1})^2/2$ therefore becomes increasingly sharply peaked about its average, with relative fluctuations being of order $\sim 1/\sqrt{L}$. Therefore, in the limit

$L \to \infty$ when we can neglect boundary terms, we can write

$$b = \frac{2\gamma}{L(2\gamma^2 + \sigma^2)}. \tag{A.6}$$

Appendix B: 5-diagonal approximation for periodic disorder

Let us have disorder only on odd sites, $\epsilon_{2j} \equiv 0$, and assume that the correlation matrix is 5-diagonal, $C_{j,j+r} \equiv 0$ for $r > 2$. The goal would be to go beyond the 3-diagonal approximation in order to describe the second resonance peak visible for instance in Figure 10. Although we will fail at that – one would need to solve at least a 11-diagonal approximation to get the second peak (which we are though not able to do analytically) – we will nevertheless correctly describe the minimum between the two peaks giving us at least some insight.

We will neglect boundary effects and solve equations in the leading order in γ/σ^2. This is justified because the second resonance maximum appears only for large σ. First, we note that because $\epsilon_{2j} = 0$ one has $h^{(3)}_{2j} = 0$. Then we also observe that $b^{(3)}_{2j+1} \sim \gamma/\sigma^2$ and can be neglected. We therefore start with the fact that $h^{(3)}$ are zero on even sites while $b^{(3)}$ are (approximately) zero on odd sites. On even sites we have $b^{(3)}_{2j} = -(h^{(2)}_{2j} - h^{(2j)}_{2j+1})/(2\gamma)$. Writing now equations for the real part of the near-diagonal at two consecutive sites in the bulk, we have

$$-2\gamma h^{(2)}_{2j} - \frac{h^{(2)}_{2j} - h^{(2)}_{2j+1}}{2\gamma} - \epsilon_{2j+1} b = 0$$
$$-2\gamma h^{(2)}_{2j+1} + \frac{h^{(2)}_{2j} - h^{(2)}_{2j+1}}{2\gamma} + \epsilon_{2j+1} b = 0.$$

From these two equations we see that only the two nearest-neighbours $h^{(2)}$ are coupled. Instead of L coupled equations we have a set of uncoupled 2×2 equations. Solving them we get

$$-h^{(2)}_{2j+1} = h^{(2)}_{2j} = -\frac{2\gamma}{(2\gamma)^2 + 2}\epsilon_{2j+1} b. \tag{B.1}$$

Inserting these into equation (A.4) we get in the thermodynamic limit $L \to \infty$,

$$b = \frac{2\gamma}{L(2\gamma^2 + \sigma^2 \frac{1}{1+1/(2\gamma^2)})}. \tag{B.2}$$

This expression correctly describes the minimum between the two peaks in Figure 10, although it fails to reproduce the left maximum.

Appendix C: Finite-size effects

Limits $L \to \infty$ and $\gamma \to 0$ do not commute. Depending on the order of the two we get either a diffusive behaviour

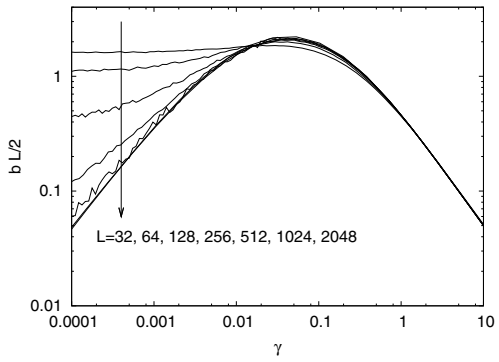

Fig. 13. Scaled particle current for $\sigma = 0.5$ and different sizes of L. Convergence to diffusive scaling, seen as an overlap of curves, is for smaller γ reached only for large sizes (data for $L = 1024$ and 2048 overlap and are indistinguishable on the scale of the plot).

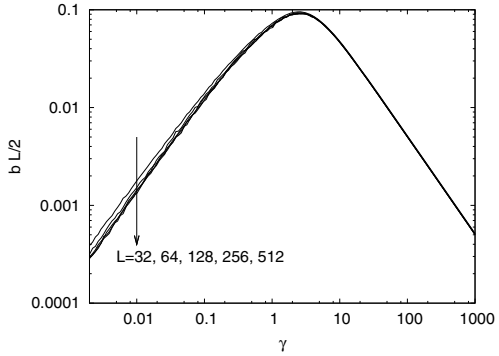

Fig. 14. Same as Figure 13, but for $\sigma = 4$. Data for $L = 128, 256, 512$ overlap.

$j \sim 1/L$ or an insulating $j \sim a^{-L}$ due to localisation. We are interested in the diffusive behaviour obtained in the correct thermodynamic limit of letting $L \to \infty$ first. In order to observe diffusive behaviour one therefore has to take sufficiently large L for each particular γ.

For instance, in Figure 13 we can see that at $\gamma = 10^{-4}$ one needs $L = 1024$ or larger, while at $\gamma = 10$ chain length $L = 32$ is enough to observe diffusive behaviour. The system size L at which diffusive behaviour is reached is smaller for larger disorder strength σ, as can be seen by comparing Figures 14 and 13.

We also note that the perturbation theory in γ around $\gamma = 0$ has a convergence radius that shrinks to zero with the system size L. The failure of a naive perturbation theory to predict diffusive behaviour at small non-zero dephasing is not very surprising because the nature of transport changes abruptly at $\gamma = 0$. Similar are problems trying to apply perturbation theory in σ in order to obtain behaviour at small σ and γ (for instance, the one in Fig. 6).

References

1. D.J. Thouless, S. Kirkpatrick, J. Phys. C **14**, 235 (1981)
2. S. Datta, *Electronic Transport in Mesoscopic Systems* (Cambridge University Press, Cambridge, 1995)
3. M. Büttiker, Phys. Rev. B **32**, 1846 (1985)

4. J.L. D'Amato, H.M. Pastawski, Phys. Rev. B **41**, 7411 (1990)
5. J. Maassen, F. Zahid, H. Guo, Phys. Rev. B **80**, 125423 (2009)
6. D. Nozaki, Y. Girard, K. Yoshizawa, J. Chem. Phys. **112**, 17408 (2008)
7. C.J. Cattena, R.A. Bustos-Marún, H.M. Pastawski, Phys. Rev. B **82**, 144201 (2010)
8. D. Nozaki, C. Gomes da Rocha, H.M. Pastawski, G. Cuniberti, Phys. Rev. B **85**, 155327 (2012)
9. R. Golizadeh-Mojarad, S. Datta, Phys. Rev. B **75**, 081301(R) (2007)
10. M. Zilly, O. Ujsághy, D.E. Wolf, Eur. Phys. J. B **68**, 237 (2009)
11. M. Zilly, O. Ujsághy, M. Woelki, D.E. Wolf, Phys. Rev. B **85**, 075110 (2012)
12. T. Stegmann, M. Zilly, O. Ujsághy, D.E. Wolf, Eur. Phys. J. B **85**, 264 (2012)
13. E. Kogan, Eur. Phys. J. B **61**, 181 (2008)
14. H. Ishii, S. Roche, N. Kobayashi, K. Hirose, Phys. Rev. Lett. **104**, 116801 (2010)
15. G. Lindblad, Commun. Math. Phys. **48**, 119 (1976)
16. V. Gorini, A. Kossakowski, E.C.G. Sudarshan, J. Math. Phys. **17**, 821 (1976)
17. M. Žnidarič, J. Stat. Mech. **2010**, L05002 (2010)
18. H.-P. Breuer, F. Petruccione, *The Theory of Open Quantum Systems* (Oxford University Press, Oxford, 2002)
19. C. Timm, Phys. Rev. B **77**, 195416 (2008)
20. M.B. Plenio, S.F. Huelga, New J. Phys. **10**, 113019 (2008)
21. P. Rebentrost, M. Mohseni, I. Kassal, S. Lloyd, A. Aspuru-Guzik, New J. Phys. **11**, 033003 (2009)
22. F. Caruso, A.W. Chin, A. Datta, S.F. Huelga, M.B. Plenio, J. Chem. Phys. **131**, 105106 (2009)
23. S. Hoyer, M. Sarovar, K.B. Whaley, New J. Phys. **12**, 065041 (2010)
24. I. Kassal, A. Aspuru-Guzik, New J. Phys. **14**, 053041 (2012)
25. M. Žnidarič, Phys. Rev. E **83**, 011108 (2011)
26. V. Eisler, J. Stat. Mech. **2011**, P06007 (2011)
27. K. Temme, M.M. Wolf, F. Verstraete, New J. Phys. **14**, 075004 (2012)
28. B. Horstmann, J.I. Cirac, G. Giedke, `arXiv:1207.1653 [quant-ph]` (2012)
29. B. Žunkovič, T. Prosen, J. Stat. Mech. **2010**, P08016 (2010)
30. T. Prosen, J. Stat. Mech. **2010**, P07020 (2010)
31. M. Žnidarič, T. Prosen, G. Benenti, G. Casati, D. Rossini, Phys. Rev. E **81**, 051135 (2010)
32. P. Jordan, E. Wigner, Z. Phys. **47**, 631 (1928)
33. P.W. Anderson, Rev. Mod. Phys. **50**, 191 (1978)
34. M. Žnidarič, New J. Phys. **12**, 043001 (2010)
35. B. Kramer, A. MacKinnon, Rep. Prog. Phys. **56**, 1469 (1993)
36. P.W. Anderson, D.J. Thouless, E. Abrahams, D.S. Fisher, Phys. Rev. B **22**, 3519 (1980)
37. H. Schomerus, M. Titov, Phys. Rev. B **67**, 100201(R) (2003)
38. L.I. Deych, M.V. Erementchouk, A.A. Lisyansky, B.L. Altshuler, Phys. Rev. Lett. **91**, 096601 (2003)
39. D.H. Dunlap, V.M. Kenkre, Phys. Rev. B **37**, 6622 (1988)
40. A.R. Kolovsky, A.V. Ponomarev, H.J. Korsch, Phys. Rev. A **66**, 053405 (2002)
41. D. Segal, A. Nitzan, W.B. Davis, M.R. Wasielewski, M.A. Ratner, J. Phys. Chem. B **104**, 3817 (2000)
42. M. Kappus, F. Wegner, Z. Phys. B **45**, 15 (1981)
43. B. Derrida, E. Gardner, J. Phys. **45**, 1283 (1984)
44. J.C. Flores, J. Phys.: Condens. Matter **1**, 8471 (1989)
45. D.H. Dunlap, H.-L. Wu, P.W. Phillips, Phys. Rev. Lett. **65**, 88 (1990)
46. G. Theodorou, M.H. Cohen, Phys. Rev. B **13**, 4597 (1976)
47. F. Delyon, H. Kunz, B. Souillard, J. Phys. A **16**, 25 (1983)
48. M. Hilke, J. Phys. A **30**, L367 (1997)
49. N. Hlubek, P. Ribeiro, R. Saint-Martin, S. Nishimoto, A. Revcolevschi, S.-L. Drechsler, G. Behr, J. Trinckauf, J.E. Hamann-Borrero, J. Geck, B. Büchner, C. Hess, Phys. Rev. B **84**, 214419 (2011)